Thermal conductivity of nano-grained $SrTiO_3$ thin films

Brian M. Foley,[1] Harlan J. Brown-Shaklee,[2] John C. Duda,[1,2] Ramez Cheaito,[1] Brady J. Gibbons,[3] Doug Medlin,[4] Jon F. Ihlefeld,[2] and Patrick E. Hopkins[1,a)]
[1]*Department of Mechanical and Aerospace Engineering, University of Virginia, Charlottesville, Virginia 22904, USA*
[2]*Sandia National Laboratories, Albuquerque, New Mexico 87185, USA*
[3]*Materials Science, School of Mechanical, Industrial, and Manufacturing Engineering, Oregon State University, Corvallis, Oregon 97331, USA*
[4]*Sandia National Laboratories, Livermore, California 94550, USA*

(Received 3 October 2012; accepted 16 November 2012; published online 6 December 2012)

We measure the thermal conductivities of nano-grained strontium titanate (ng-$SrTiO_3$) films deposited on sapphire substrates via time-domain thermoreflectance. The 170 nm thick oxide films of varying grain-size were prepared from a chemical solution deposition process. We find that the thermal conductivity of ng-$SrTiO_3$ decreases with decreasing average grain size and attribute this to increased phonon scattering at grain boundaries. Our data are well described by a model that accounts for the spectral nature of anharmonic Umklapp scattering along with grain boundary scattering and scattering due to the film thickness. © *2012 American Institute of Physics*.
[http://dx.doi.org/10.1063/1.4769448]

Potential applications for thermoelectric (TE) devices in areas such as waste-energy scavenging and solid-state thermal management have made the engineering of TE materials an important area of research. Advancements in materials and processing techniques have paved the way to produce scalable, cost effective materials with desirable properties for an effective TE device.[1] As these material systems are created, their potential as a viable TE material is evaluated based on their thermoelectric figure of merit, denoted ZT, given by $S^2\sigma T/\kappa$, where S is the Seebeck coefficient, σ is the electrical conductivity, κ is the thermal conductivity, and T is the absolute temperature. Nanosystems have shown promise as potential high ZT materials due to the ability to engineer electrical properties somewhat separately from the thermal and phonon properties at this scale. However, effectively increasing ZT from individual nanosystems to "device-ready" scales has proven to be a complicated challenge due to the inefficient scaling of these electronic and phononic mechanisms and properties.

Transition-metal oxides have garnered significant attention as potentially scalable TE material solutions due to their non-toxicity, stability, and high abundance in the earth's crust. In particular, $SrTiO_3$ is a transition-metal oxide with several properties that may make it a candidate for TE devices of the future. This large band-gap perovskite oxide can be doped on both the A and B cationic sites or with oxygen vacancies to increase the n-type carrier concentration. In addition, the large orbital degeneracy of the titanium d-band carriers results in power factors ($S^2\sigma$) that compare quite well with the current state-of-the-art.[2] It has been shown that increasing the n-type carrier concentration via the aforementioned methods can improve the power factor of the material with minimal effect on the thermal conductivity, consequently causing an increase in ZT.[2] Furthermore, the thermal conductivity of $SrTiO_3$ decreases with increasing temperature due to the increase in anharmonic phonon-phonon scattering at higher temperatures. Together, these trends yield a maximum ZT between 700 and 900 K, thus making $SrTiO_3$ an attractive candidate for waste-energy scavenging in high temperature applications (e.g., cogeneration plants, satellite power sources, automobile exhaust recovery systems, etc.).[3,4]

In addition to augmenting the electronic properties of TE materials through doping, a great deal of research has focused on improving ZT by reducing the thermal conductivity of materials via nanostructuring, a thorough review of which can be found in Refs. 5–7. Although these approaches have exhibited promise in creating materials with high thermoelectric figures of merit, the scalability of some of these materials is lacking due to their intensive fabrication processes.[8] Alternatively, bulk nanostructured materials, or nanocomposites, may be produced in large quantities both quickly and inexpensively.[8] The ability of producing nanocomposite $SrTiO_3$ over large surfaces is crucial for successful thermoelectric device-commercialization with this material. This would also impact other applications requiring materials that are stable at high temperatures, such as thermal barrier coatings in turbine blades and heat shielding in high-atmosphere or outer-space vehicles.

Clearly, an understanding of the size-dependent phonon scaling mechanisms contributing to the thermal conductivity of $SrTiO_3$ nanocomposites will benefit an array of potential applications. In turn, a well-developed knowledge of the thermal properties of nanostructured $SrTiO_3$ is critical. In this work, we measure the thermal conductivity, κ, of nanocrystalline $SrTiO_3$ films with varied average grain sizes (which we refer to as nanograined $SrTiO_3$ or ng-$SrTiO_3$), fabricated through chemical solution deposition (CSD). CSD is an inexpensive and scalable technique for producing ng-$SrTiO_3$ over large areas with a high degree of repeatability.[9] Using time-domain thermoreflectance (TDTR), we measure the thermal conductivities of ng-$SrTiO_3$ thin films of varying grain size. We show that the thermal conductivity of ng-$SrTiO_3$ decreases as the average grain sizes get smaller. We

a)Electronic mail: phopkins@virginia.edu.

present a model that incorporates the effect of grain size by means of a boundary scattering term that accounts for the spectral nature of the phonon mean free paths in strontium titanate.

The strontium titanate films were prepared via chemical solution deposition using a chelate chemistry based on previous work.[10,11] Briefly, anhydrous strontium acetate was dissolved in propionic acid (0.25 M) at room temperature with constant stirring. Separately, titanium isopropoxide was chelated with one molar equivalent of 2,4-pentanedione and mixed at room temperature to create a stable titanium precursor solution. A stoichiometric amount of the strontium acetate solution was added to the titanium precursor solution and then diluted to a final concentration of 0.15 M with methanol.

The solution was spin cast at 3000 RPM for 30 sec onto a 50 mm diameter (0001)-oriented single crystalline Al_2O_3 wafer (Union Carbide, UCC Crystal Products) and subsequently pyrolyzed at 300 °C for 3 min on a hotplate. Pyrolyzed films were heated at 20 °C/min to 700 °C for 30 min in air to crystallize the $SrTiO_3$ film. An every-layer firing approach was used to ensure high-density films,[12] where the process of spin casting, pyrolysis, and crystallization from the same precursor solution was repeated nine times to produce nominally 170 nm thick films. After crystallization, the wafer was diced to form 1 cm^2 coupons that could be individually heat treated at 700, 800, 900, or 1000 °C for 30 min to modify the final grain size.[13]

Phase assemblage and crystallinity of the $SrTiO_3$ films were confirmed by x-ray diffraction (Philips MPD) using Cu K_α radiation in standard Bragg-Brentano geometry. Cross-sectional and plan-view microstructural images (Fig. 1) were obtained by scanning electron microscopy (SEM, Zeiss, Gemini Supra 55VP). Average grain size measurements were determined from film plan view images using the linear intercept method[14] and the results are summarized in Table I where d_{avg} is the average grain size and σ_d is the associated uncertainty in the measured value. Transmission electron microscopy (TEM) and spectroscopic ellipsometry (SE, V-VASE from J. A. Woollam) were used to verify density of the films. Porosity was extracted from SE measurements via modeling the ng-$SrTiO_3$ layer as a mixture of void and $SrTiO_3$ using a Bruggeman effective medium approximation. Porosity levels of less than 13.5% were observed for films prepared at 700 °C (sample A) and decreased to 9.3% for films processed at 1000 °C for 30 min (sample F). Finally, aluminum films nominally 90 nm thick were e-beam evaporated onto the samples in order to serve as transducers for subsequent TDTR scans. The precise thicknesses of the Al films were determined via picosecond ultrasonic measurements during TDTR scans.[15,16]

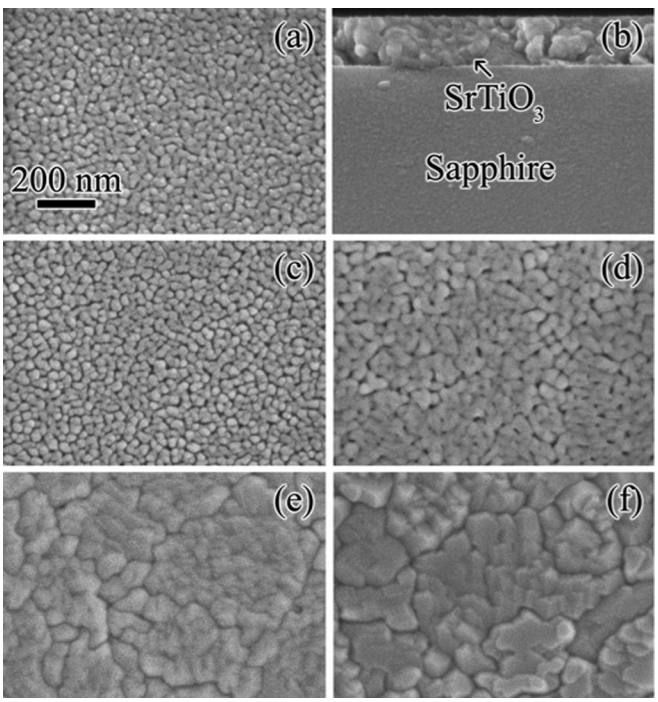

FIG. 1. (a) Plan and (b) cross sectional SEM micrographs of as crystallized SrTiO3 films on (0001) sapphire. Plan view images of films that were post annealed at (c) 700, (d) 800, (e) 900, and (f) 1000 °C demonstrate the degree to which post crystallization anneals impact the film microstructures.

The thermal conductivities of the ng-$SrTiO_3$ films were determined using TDTR[17] by fitting the data to a multi-layer thermal model that has been detailed by several groups elsewhere.[18–20] For this study, we modulate the pump path at 11.39 MHz with a linearly amplified sinusoid and monitor the ratio of the in-phase to out-of-phase signal of the probe beam with a lock-in amplifier. We assume literature values for the heat capacities of the Al film[21] and Al_2O_3 substrate,[22,23] as well as the heat capacity of the $SrTiO_3$ (Ref. 24) which we then reduce according to the measured density to account for the porosity. The thermal conductivity of the Al is approximated from previous measurements of Al films evaporated under identical conditions,[18] although over the time delay of our TDTR measurements, we are relatively insensitive to the thermal conductivity of the Al. We fit the TDTR model to the data by varying the thermal conductivity of the ng-$SrTiO_3$ films and the thermal boundary conductance between the Al and the ng-$SrTiO_3$ samples. We are generally more sensitive to the thermal conductivities of the ng-$SrTiO_3$ films due to their low conductivity. In addition, due to the thickness of the samples and their relatively low thermal conductivity compared to the thermal penetration depth of our laser at 11.39 MHz, we are relatively insensitive to the thermal boundary conductance between the ng-$SrTiO_3$ and the Al_2O_3 substrate. However, to ensure accuracy in our experimental data of κ for the ng-$SrTiO_3$, we conduct TDTR measurements at different frequencies to determine the thermal properties of the ng-$SrTiO_3$/Al_2O_3 interface and the thermal conductivity of the Al_2O_3 (Refs. 25–27). We then

TABLE I. Annealing conditions (temperature, treatment time) and the resulting average grain sizes (d_{avg}) and measurement uncertainties (σ_d).

Sample	Anneal temperature (° C)	Treatment time (min)	d_{avg} (nm)	σ_d (nm)
A	700	0	28.3	2.4
B	700	30	31.3	3.3
C	800	30	45.5	3.6
D	900	30	59.9	4.8
E	1000	5	64.1	3.8
F	1000	30	88.1	14.1

use these values in our TDTR analysis to determine the thermal conductivity of ng-$SrTiO_3$. Finally, due to the time scale on which the TDTR measurements are made, our measurements are only sensitive to the $SrTiO_3$ network material and not the effective composite.[28] Porosity only influences the heat capacity adjustments used to calculate thermal conductivity with the TDTR technique, whereas the calculated diffusivity values are intrinsic to the network material and not the network-pore composite. This fact makes TDTR unique from other diffusivity measurements such as the laser flash techniques which sample the volume of a network and the accompanying porosity to arrive at an effective composite thermal conductivity.

Figure 2 shows the measured thermal conductivities of these ng-$SrTiO_3$ films as a function of average grain size. In addition, we plot the data of Wang *et al.* from Ref. 29 and the thermal conductivity of bulk $SrTiO_3$ (Refs. 30 and 31). The error bars represent the uncertainty calculated due to the Al film thickness and the standard deviation about the mean of the three measurements on each sample. In our nanograined samples, we find that there is a 50% to 60% reduction in thermal conductivity from the bulk value for $SrTiO_3$ at room temperature. Furthermore, the data exhibit the trend that the thermal conductivity decreases with decreasing average grain size. We attribute the majority of the observed reduction in thermal conductivity to be due to phonon-grain boundary scattering since the change in porosity will only decrease the thermal conductivity by less than 5% as approximated by differential effective medium theories for thermal transport.[32,33] Wang *et al.* reported similar behavior in their thermal conductivity measurements of $SrTiO_3$ pellet ceramics made with spark plasma sintering (SPS); however, their reported thermal conductivities are slightly higher than ours measured with TDTR. Since the grain sizes are smaller than the film thickness, we rule out film thickness size effects as the cause of this difference, as we quantitatively interrogate with the model described below. We are therefore uncertain of the sources of this slight discrepancy at this time.

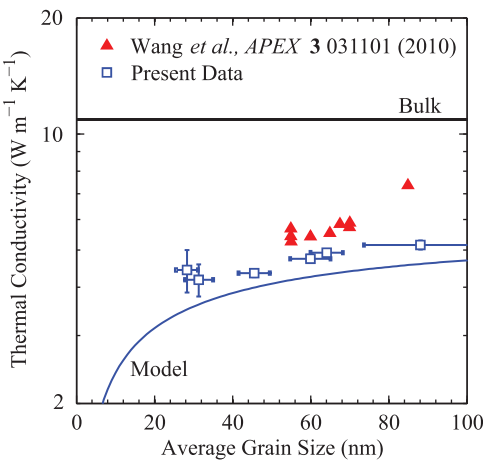

FIG. 2. Thermal conductivity of ng-$SrTiO_3$ as a function of average grain size (hollow squares), along with the previous data of Wang *et al.* (filled triangles) and bulk $SrTiO_3$ (solid line). In addition, we plot the prediction of Eq. (1), which is shown to agree well with our data. The agreement between our model and data suggests that the frequency dependence of the phonon mean free paths in $SrTiO_3$ must be taken into account to properly account for the thermal conductivity reduction due to grain boundary scattering.

The model shown in Fig. 2 was calculated using the following expression

$$\kappa = \frac{1}{3}\sum_j C_{v,j} v_j^2 \tau_j = \frac{1}{6\pi^2}\sum_j \int_k \hbar\omega_j \frac{\partial f_{BE}}{\partial T} v_j^2 \tau_j k^2 dk, \quad (1)$$

where κ is the thermal conductivity, j is the phonon polarization index, C_v is the volumetric heat capacity, v is the phonon group velocity, τ is the total scattering time, ω is the angular frequency, $\partial f_{BE}/\partial T$ is the temperature derivative of the Bose-Einstein distribution function, and k is the phonon wavevector. In the derivation of the right-most expression in Eq. (1), we have assumed an isotropic Brillouin zone, which is reasonable given the high symmetry (space group $Pm\bar{3}m$) of $SrTiO_3$. For $SrTiO_3$, we take the experimentally determined dispersion in the [100] direction from Cowley[34] by fitting each of the 15 phonon branches with fourth-order polynomials. We take the total scattering time, τ_j, as the combination of the scattering times due to both anharmonic phonon-phonon (τ_a), and phonon-grain boundary (τ_{gb}), and phonon-film boundary (τ_{fb}) scattering. It should be noted that additional contributions to the reduction in thermal conductivity likely include phonon scattering at internal pore boundaries, which would follow the same dependence as grain boundary scattering. However, since TDTR cannot distinguish between grain boundary scattering and scattering at other internal interfaces, we lump this together as a single boundary scattering term. The total scattering rate is then determined through Matthiessen's rule,[35] given as

$$\tau_j = \left[\frac{1}{\tau_a} + \frac{1}{\tau_{gb}} + \frac{1}{\tau_{fb}}\right]^{-1} = \left[BT\omega_j^2 \exp\left(-\frac{C}{T}\right) + \frac{v_j}{d_{avg}} + \frac{v_j}{170\times10^{-9}}\right]^{-1}, \quad (2)$$

where d_{avg} is the average grain size presented in Table I and the last term represents scattering due to the film thickness. The constants B and C are determined by fitting Eq. (1) to temperature-dependent experimental data for bulk $SrTiO_3$ (Refs. 24 and 36); we find $B = 6.8\times10^{-19}\,\mathrm{s\,K^{-1}}$ and $C = 40\,\mathrm{K}$. In Eq. (2), we see that for large grain sizes (approaching single-crystalline films), τ_a is the dominant scattering mechanism. As d_{avg} decreases, the relative contribution of τ_{gb} to the total scattering time increases, causing a reduction in the thermal conductivity of the associated films. We find only a minor dependency of our model on film thickness, and the film thickness scattering term only leads to a 20% decrease in the predicted thermal conductivity at the largest grain sizes. This alludes to the fact that the sources of the difference between our data (open squares) and Wang's data (filled triangles) are not due to film size effects.

Our experimental data agree quite well with the model, suggesting that the scattering mechanisms presented in Eq. (2) accurately describe the phonon physics occurring in the ng-$SrTiO_3$ films. This is in stark contract with the model presented by Wang *et al.*,[24] in which a gray medium was assumed in the $SrTiO_3$ and they described their data by considering a Kapitza conductance across the grain boundaries. In general, gray approximations to thermal conductivity and Kapitza conductance over-estimate the thermal transport

processes due to the decrease in phonon velocities and increase in phonon scattering rates in the dispersive modes near the Brillouin zone edge.[37–39] If phonon scattering is not dominated by grain boundary scattering, then anharmonic phonon scattering must be accounted for in the thermal conductivity model. This is due to the strong spectral dependence of these Umklapp processes and their interplay with grain boundary scattering at different phonon frequencies. Therefore, using the Kapitza conductance approach to analyze experimental data in this regime, due to its gray body "series resistor" interpretation of thermal conduction, would not properly account for this interplay. In addition, as ng-$SrTiO_3$ is clearly still in an Umklapp dominated regime for these grain sizes, as shown by Wang *et al.*,[24] the grain boundary Kapitza conductance cannot be accurately inferred from experimental data since larger thermal resistances and thereby temperature drops occur in the grain, not across the grain boundary. However, for material systems in which the thermal conductivity is dominated by grain boundary scattering (based on the temperature trends), the grain boundary Kapitza conductance could be inferred from experimental data (e.g., nanocrystalline yttria-stabilized zirconia[40] or polycrystalline silicon[41,42]).

In conclusion, we have investigated the effects of grain boundary scattering on the thermal conductivity of nanograined $SrTiO_3$. We find a controlled decrease in thermal conductivity of the ng-$SrTiO_3$ for grain sizes from ~30 to 90 nm. Our data are well described by a model that accounts for the spectral nature of anharmonic Umklapp scattering along with grain boundary scattering and scattering due to the film thickness.

The authors would like to thank Bonnie McKenzie for providing SEM images. The authors are grateful for support from the National Science Foundation Grant No. CBET 1134311 (U.V.). This work was performed in part at the Center for Atomic, Molecular, and Optical Science (CAMOS) at the University of Virginia. This work was supported, in part, by the Laboratory Directed Research and Development (LDRD) program at Sandia National Laboratories. Sandia National Laboratories is a multi-program laboratory managed and operated by Sandia Corporation, a wholly owned subsidiary of Lockheed Martin Corporation, for the U.S. Department of Energy's National Nuclear Security Administration under contract DE-AC04-94AL85000.

[1]G. J. Snyder and E. S. Toberer, Nature Mater. **7**, 105 (2008).
[2]J. Ravichandran, W. Siemons, D. W. Oh, J. T. Kardel, A. Chari, H. Heijmerikx, M. L. Scullin, A. Majumdar, R. Ramesh, and D. G. Cahill, Phys. Rev. B **82**, 165126 (2010).
[3]L. E. Bell, Science **321**, 1457 (2008).
[4]C. B. Vining, Nature Mater. **8**, 83 (2009).
[5]C. J. Vineis, A. Shakouri, A. Majumdar, and M. G. Kanatzidis, Adv. Mater. **22**, 3970 (2010).
[6]K. Koumoto, I. Terasaki, and R. Funahashi, MRS Bull. **31**, 206 (2006).
[7]K. Koumoto, Y. Wang, R. Zhang, A. Kosuga, and R. Funahashi, Annu. Rev. Mater. Res. **40**, 363 (2010).
[8]A. J. Minnich, M. S. Dresselhaus, Z. F. Ren, and G. Chen, Energy Environ. Sci. **2**, 466 (2009).
[9]G. L. Brennecka, J. F. Ihlefeld, J.-P. Maria, B. A. Tuttle, and P. G. Clem, J. Am. Ceram. Soc. **93**, 3935 (2010).
[10]S. Hoffmann and R. Waser, J. Eur. Ceram. Soc. **19**, 1339 (1999).
[11]R. W. Schwartz, P. G. Clem, J. A. Voigt, E. R. Byhoff, M. Van Stry, T. J. Headley, and N. A. Missert, J. Am. Ceram. Soc. **82**, 2359 (1999).
[12]S. M. Aygun, J. F. Ihlefeld, W. J. Borland, and J.-P. Maria, J. Appl. Phys. **109**, 034108 (2011).
[13]J. F. Ihlefeld, A. M. Vodnick, S. P. Baker, W. J. Borland, and J.-P. Maria, J. Appl. Phys. **103**, 074112 (2008).
[14]E-112-96, *Standard Test Methods for Determining Average Grain Size* (ASTM International, 2003), Vol. 03.01.
[15]C. Thomsen, J. Strait, Z. Vardeny, H. J. Maris, J. Tauc, and J. J. Hauser, Phys. Rev. Lett. **53**, 989 (1984).
[16]C. Thomsen, H. T. Grahn, H. J. Maris, and J. Tauc, Phys. Rev. B **34**, 4129 (1986).
[17]D. G. Cahill, K. Goodson, and A. Majumdar, J. Heat Transfer **124**, 223 (2002).
[18]P. E. Hopkins, J. R. Serrano, L. M. Phinney, S. P. Kearney, T. W. Grasser, and C. T. Harris, J. Heat Transfer **132**, 081302 (2010).
[19]A. J. Schmidt, X. Chen, and G. Chen, Rev. Sci. Instrum. **79**, 114902 (2008).
[20]D. G. Cahill, Rev. Sci. Instrum. **75**, 5119 (2004).
[21]Y. Touloukian and E. Buyco, *Thermophysical Properties of Matter - Specific Heat: Metallic Elements and Alloys* (IFI/Plenum, New York, 1970), Vol. 4.
[22]Y. S. Touloukian, R. W. Powell, and C. Y. Ho, *Thermophysical Properties of Matter - Thermal Conductivity: Nonmetallic Solids* (IFI/Plenum, New York, 1970), Vol. 2.
[23]Y. S. Touloukian and E. H. Buyco, *Thermophysical Properties of Matter - Specific Heat: Nonmetallic Solids* (IFI/Plenum, New York, 1970), Vol. 5.
[24]H. C. Wang, C. L. Wang, W. B. Su, J. Liu, Y. Zhao, H. Peng, J. L. Zhang, M. L. Zhao, J. C. Li, N. Yin, and L. M. Mei, Mater. Res. Bull. **45**, 809 (2010).
[25]P. E. Hopkins, J. C. Duda, S. P. Clark, C. P. Hains, T. J. Rotter, L. M. Phinney, and G. Balakrishnan, Appl. Phys. Lett. **98**, 161913 (2011).
[26]N. C. Shukla, H.-H. Liao, J. T. Abiade, F. Liu, P. K. Liaw, and S. T. Huxtable, Appl. Phys. Lett. **94**, 081912 (2009).
[27]S. T. Huxtable, D. G. Cahill, and L. M. Phinney, J. Appl. Phys. **95**, 2102 (2004).
[28]P. E. Hopkins, B. Kaehr, E. S. Piekos, D. Dunphy, and C. J. Brinker, J. Appl. Phys. **111**, 113532 (2012).
[29]Y. Wang, K. Fujinami, R. Zhang, C. Wan, N. Wang, Y. Ba, and K. Koumoto, Appl. Phys. Express **3**, 031101 (2010).
[30]Y. Suemune, J. Phys. Soc. Jpn. **20**, 174 (1965).
[31]C. Yu, M. L. Scullin, M. Huijben, R. Ramesh, and A. Majumdar, Appl. Phys. Lett. **92**, 191911 (2008).
[32]R. M. Costescu, A. J. Bullen, G. Matamis, K. E. O'Hara, and D. G. Cahill, Phys. Rev. B **65**, 094205 (2002).
[33]D. A. G. Bruggeman, Ann. Phys. **416**, 636 (1935).
[34]R. A. Cowley, Phys. Rev. **134**, A981 (1964).
[35]C. Kittel, *Introduction to Solid State Physics*, 7th ed. (John Wiley and Sons, Inc., 1996).
[36]D.-W. Oh, J. Ravichandran, C.-W. Liang, W. Siemons, B. Jalan, C. M. Brooks, M. Huijben, D. G. Schlom, S. Stemmer, L. W. Martin, A. Majumdar, R. Ramesh, and D. G. Cahill, Appl. Phys. Lett. **98**, 221904 (2011).
[37]J. C. Duda, T. E. Beechem, J. L. Smoyer, P. M. Norris, and P. E. Hopkins, J. Appl. Phys. **108**, 073515 (2010).
[38]A. Ward and D. A. Broido, Phys. Rev. B **81**, 085205 (2010).
[39]J. D. Chung, A. J. H. McGaughey, and M. Kaviany, J. Heat Transfer **126**, 376 (2004).
[40]H.-S. Yang, G. R. Bai, L. J. Thompson, and J. A. Eastman, Acta Mater. **50**, 2309 (2002).
[41]Z. Wang, J. E. Alaniz, W. Jang, J. E. Garay, and C. Dames, Nano Lett. **11**, 2206 (2011).
[42]S. Uma, A. D. McConnell, M. Asheghi, K. Kurabayashi, and K. E. Goodson, Int. J. Thermophys. **22**, 605 (2001).